JACS
JOURNAL OF THE AMERICAN CHEMICAL SOCIETY

ARTICLE

pubs.acs.org/JACS

Hierarchical Chiral Expression from the Nano- to Mesoscale in Synthetic Supramolecular Helical Fibers of a Nonamphiphilic C_3-Symmetrical π-Functional Molecule

Ion Danila,[§] François Riobé,[§,†] Flavia Piron,[§] Josep Puigmartí-Luis,[†] John D. Wallis,[¶] Mathieu Linares,[‡] Hans Ågren,[‡] David Beljonne,[#] David B. Amabilino,*[,†] and Narcis Avarvari*[,§]

[§]Université d'Angers, CNRS, Laboratoire MOLTECH-Anjou, UMR 6200, UFR Sciences, Bât. K, 2 Bd. Lavoisier, 49045 Angers, France

[†]Institut de Ciència de Materials de Barcelona (CSIC), Campus Universitari de Bellaterra, 08193 Cerdanyola del Vallès, Catalonia, Spain

[¶]School of Science and Technology, Nottingham Trent University, Clifton Lane, Nottingham, NG11 8NS, United Kingdom

[‡]Laboratory of Theoretical Chemistry, Royal Institute of Technology, SE-106 91 Stockholm, Sweden

[#]Laboratory for Chemistry of Novel Materials, Université de Mons, Place du Parc 20, 7000 Mons, Belgium

Supporting Information

ABSTRACT: The controlled preparation of chiral structures is a contemporary challenge for supramolecular science because of the interesting properties that can arise from the resulting materials, and here we show that a synthetic nonamphiphilic C_3 compound containing π-functional tetrathiafulvalene units can form this kind of object. We describe the synthesis, characterization, and self-assembly properties in solution and in the solid state of the enantiopure materials. Circular dichroism (CD) measurements show optical activity resulting from the presence of twisted stacks of preferential helicity and also reveal the critical importance of fiber nucleation in their formation. Molecular mechanics (MM) and molecular dynamics (MD) simulations combined with CD theoretical calculations demonstrate that the (*S*) enantiomer provides the (*M*) helix, which is more stable than the (*P*) helix for this enantiomer. This relationship is for the first time established in this family of C_3 symmetric compounds. In addition, we show that introduction of the "wrong" enantiomer in a stack decreases the helical reversal barrier in a nonlinear manner, which very probably accounts for the absence of a "majority rules" effect. Mesoscopic chiral fibers, which show inverted helicity, i.e. (*P*) for the (*S*) enantiomer and (*M*) for the (*R*) one, have been obtained upon reprecipitation from dioxane and analyzed by optical and electronic microscopy. The fibers obtained with the racemic mixture present, as a remarkable feature, opposite homochiral domains within the same fiber, separated by points of helical reversal. Their formation can be explained through an "oscillating" crystallization mechanism. Although C_3 symmetric disk-shaped molecules containing a central benzene core substituted in the 1,3,5 positions with 3,3′-diamido-2,2′-bipyridine based wedges have shown peculiar self-assembly properties for amphiphilic derivatives, the present result shows the benefits of reducing the nonfunctional part of the molecule, in our case with short chiral isopentyl chains. The research reported herein represents an important step toward the preparation of functional mesostructures with controlled helical architectures.

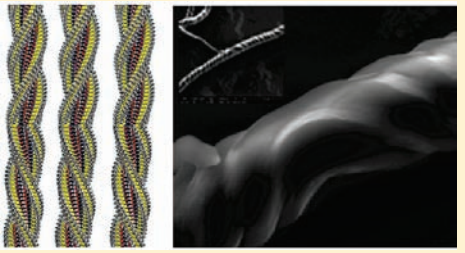

INTRODUCTION

Supramolecular chirality expressed through the formation of helical fibres of nano- or meso-scopic size following hierarchical self-assembly processes is a topic of great current interest in diverse scientific fields.[1−4] Various applications such as chiral recognition, when the fibers are entrapped in gels,[5] asymmetric synthesis,[6] using silica inorganic helices obtained by replication of organic helical fibers,[7] helical crystallization of biological macromolecules, when the chiral fibers serve as a template,[8,9] biocompatible scaffolds for imaging, tissue engineering, and drug delivery, in the case of nanofibers decorated with bioactive molecules,[10] have been extensively investigated in the past 15 years. However, probably the most promising applications of chiral supramolecular structures lie in the field of materials, either inorganic, prepared upon a transcription process starting from organic fibers,[11−13] or organic, when a functional group appended to the molecular building block possesses a specific property which can be then replicated and amplified at the nano- or mesoscale of the chiral aggregate.[14−17] Moreover, collective properties, not observed in the isolated building blocks, can often emerge in the supramolecular assemblies. Many of the systems involved in the formation of chiral fibers consist in π-conjugated derivatives, such as phenylene-vinylenes,[18−20] oligothiophenes,[21,22] and hexabenzocoronenes,[23,24] well-known for their semiconducting behaviors, thus providing twisted or helical wires or ribbons, with conducting properties.[25] The ultimate goal of this approach is to integrate such fibers in molecular electronic devices.[26,27]

Received: March 10, 2011
Published: April 25, 2011

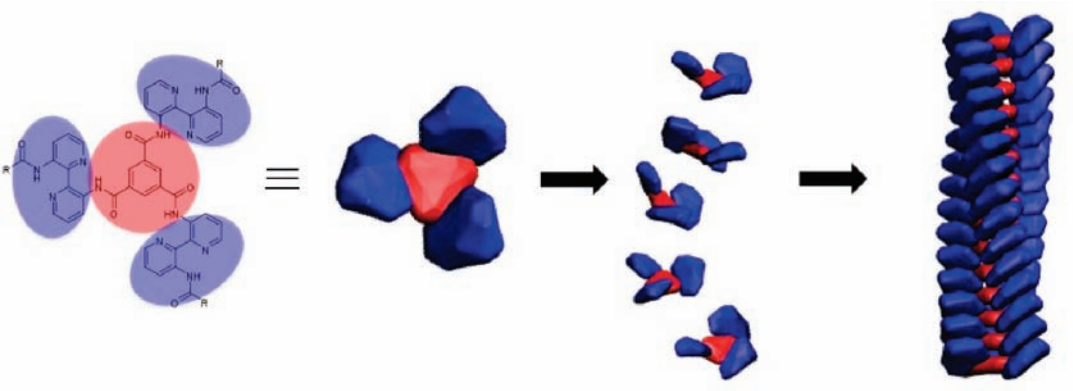

Figure 1. Schematic model of the self-assembly of twisted stacks of C_3 symmetric *N*,*N*′,*N*″-Tris[3(3′-carbamoylamino)-2,2′-bipyridyl]-benzene-1,3,5-tricarbonamide derivatives.

It is generally well established that formation of supramolecular aggregates occurs through a bottom-up process, involving cooperative intermolecular forces such as $\pi-\pi$ stacking and hydrogen bonding, combined with other weaker and nondirectional interactions,[14−17,26,27] very often leading to fibers possessing complex superstructures. Moreover, it has been emphasized that the presence of chiral alkyl chains at the periphery of the molecule which engage in the self-assembly process can trigger the preferential formation of only one helicity, as an expression of hierarchical organization at different levels. In this respect, a very interesting building block provided with C_3 symmetry, consisting of a central aromatic ring functionalized at the 1, 3, and 5 positions with substituted *N*-monoacylated 3,3′-diamino-2,2′-bipyridine units, has been introduced by Meijer and co-workers (Figure 1).[28] Because of the steric hindrance around the central aromatic core, the three bipyridine wedges, self-rigidified through intramolecular hydrogen bonding, adopt a propeller-like conformation, and furthermore, the interplay of the $\pi-\pi$ stacking interactions lead to the establishment of columnar stacks with a helical supramolecular architecture.[29,30]

The substituents (R in Figure 1) attached to the bipyridine units generally consist of 3,4,5-trialkoxy-benzene fragments containing solubilizing alkyl[28,31,32] or polyether chains.[29] More recently, even desymmetrization of this platform has been achieved, by the use of two different substituents, two at selected positions and the other at the remaining one.[33] Depending on the substituents and preparation conditions, discotic liquid crystals[28,33,34] or gels[30] have been obtained. In the case of the aggregates containing chiral side chains, the occurrence of helical stacks has been proven by circular dichroism (CD) spectroscopic studies in solution,[35] which also emphasized nonlinear effects in the chiral induction[36] according to "sergeants-and-soldiers"[31] and "majority rules"[32] principles. The peculiar self-assembly properties of this platform prompted us to attach to its periphery π-functional tetrathiafulvalene (TTF) units, a well-known electron rich donor,[37,38] in order to take advantage of the propensity of TTF derivatives to engage in intermolecular S···S contacts, a very important feature of their solid state structures. Thus, by the use of the C_3 compound containing three achiral bis(thioethyl)-TTF fragments, we have recently prepared electroactive nanowires from gels, which had shown electric conductivity upon doping with iodine.[39] Several TTF based gelators that give electroactive fibers upon doping have been described in the past five years,[40−46] but chiral expression has been only evidenced[47] by electron microscopy at the nanoscale. We anticipated that the presence of chiral alkyl chains on the lateral sulfur atoms would induce a preferential helicity in the successive levels of hierarchical organization of the supramolecular aggregates of our C_3 symmetric derivatives. However, we made the choice to use rather short chains in order to avoid phase segregation and to favor intermolecular TTF···TTF contacts between the primary helical stacks with the hope to access higher levels of self-assembly.

We describe here the synthesis and characterization of both enantiomers of the C_3 symmetric tris[3(3′-carbamoylamino)-2,2′-bipyridyl]-benzene-1,3,5-tricarbonamide derivatives containing three chiral bis[(*R*) or (*S*)-2-methylbutylthio]-tetrathiafulvalenyl units at the periphery. Their self-assembly properties are investigated in solution by variable temperature circular dichroism (CD) measurements, combined with theoretical calculations, in order to determine the sense of helicity of the aggregates. The preference for a helical twist over the opposite one for each enantiomer is strongly supported by unprecedented molecular mechanics (MM) and molecular dynamics (MD) simulations in this family of disk shaped compounds, at two successive hierarchical levels. The mesoscopic size fibers obtained in the solid state from the pure enantiomers, showing preferential helical coiling and very interesting hierarchical architectures, are analyzed by optical and electron microscopy. Moreover, the racemic system, providing fibers with remarkable morphology which provide key insight into the chiral induction in this system, is also described.

RESULTS AND DISCUSSION

Synthesis and Characterization. For the synthesis of the enantiomeric disk-shaped compounds **1a** (*S*,*S*,*S*,*S*,*S*,*S*) and **1b** (*R*,*R*,*R*,*R*,*R*,*R*) we have applied the convergent procedure described previously,[39] by using the appropriate TTF acid chlorides **2a** and **2b**, obtained from the corresponding diesters **8a** and **8b**, containing chiral 2-methyl-butyl chains introduced in the early stage of the synthesis (Schemes 1 and 2; see Supporting Information for details of the synthesis of all the precursors). While for the preparation of the (*S*,*S*) enantiomer **8a** the commercially available (*S*)-1-bromo-2-methyl-butane was used, the (*R*,*R*) enantiomer **8b** required first the synthesis of (*R*)-1-bromo-2-methyl-butane through a six-step procedure[48−50] adapted from literature (see Supporting Information for experimental details).

dx.doi.org/10.1021/ja202211k |*J. Am. Chem. Soc.* 2011, 133, 8344–8353

Scheme 1. Synthesis of the TTFs 2a and 2b

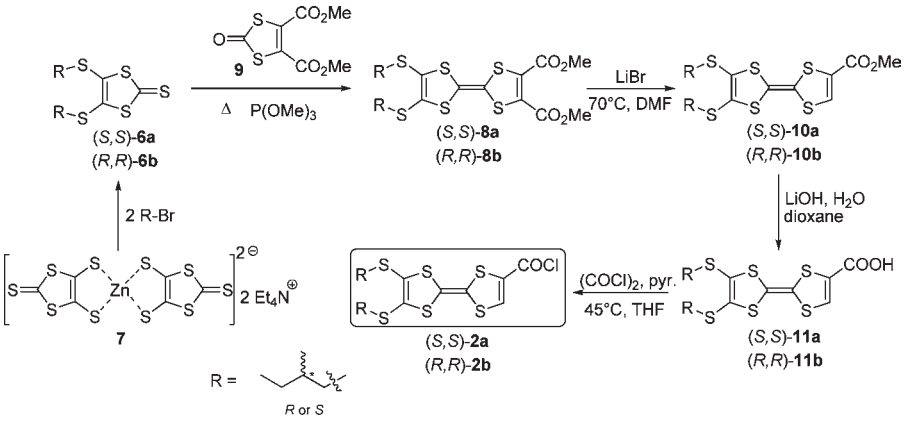

Scheme 2. Synthesis of the C_3-Symmetric Enantiopure Tris(TTF) 1a and 1b

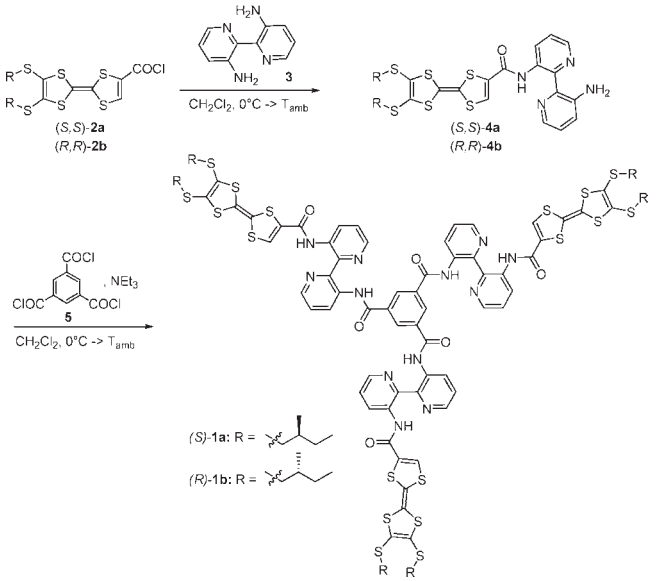

The enantiomeric acid chlorides **2a**−**b** were selectively reacted with 1 equiv of 3,3′-diamino-2,2′-bipyridine **3**,[51] to obtain the monoacylated derivatives **4a**−**b** in good isolated yields, with only traces of the bis(TTF) compounds being separated. Subsequent reaction of **4a**−**b** with trimesic chloride **5** afforded **1a**−**b** in 85% yield, as red-brownish powders which are soluble in chlorinated solvents. For example, viscous solutions are obtained at high concentrations of compound in methylene chloride, yet the gel state has not been reached, as was the case with the achiral ethyl substituents,[39] perhaps because of the greater solubility of these new chiral derivatives. Although ^{1}H NMR spectra show only broad signals even at high dilutions in $CDCl_3$, yet corresponding to the different functional groups, mass spectrometry and elemental analysis are in agreement with the proposed tris(TTF) structure.

Investigation of Aggregation by Circular Dichroism Spectroscopy. A very powerful technique to study helical supramolecular aggregates in solution is circular dichroism (CD) spectroscopy.[35] Our system as an isolated molecule is not CD active in the usual UV−visible range, since the chiral isopentyl chains do not absorb there, and their influence on the chromophore transitions (and by inference the conformation of the molecule) is negligible. This assumption has been verified by the absence of any bands in the CD spectra of either enantiomer of **1** in methylene chloride or chloroform, solvents which do not favor their self-assembly. The UV−visible spectrum of **1** in CH_2Cl_2 ($c = 10^{-5}$ M; see Supporting Information) shows, in the long wavelength region, absorption bands attributable to both the bipyridine and TTF chromophores, arising from $\pi-\pi^*$ transitions. Accordingly, the less energetic absorption that appears as a broad, weak band, at $\lambda_{max} = 450$ nm ($\varepsilon = 7400$ L mol^{-1} cm^{-1}), can be attributed to a typical $\pi_{HOMO} - \pi_{LUMO}^*$ transition in TTF-amides.[52] Then, a much more intense and broad band, as a result of several closely lying transitions, is observed between 400 and 270 nm with a λ_{max} of 296 nm ($\varepsilon = 74000$ L mol^{-1} cm^{-1}). The shoulders at 380 and 359 nm are assigned to bipyridine transitions, by comparison with the Eindhoven system,[31,32] while the one at 326 nm very probably arises from the TTF-amide units. The spectrum in dioxane, a solvent in which the compound is sufficiently soluble at room temperature to allow accurate measurements ($c = 2-5 \times 10^{-5}$ M, after moderate heating to help solubilization), presents the same features, with the maxima of the absorption bands slightly blue-shifted by a few nanometers. Nevertheless, strong optical activity is observed in the CD spectra in this solvent, with the expected mirror image relationship for the two enantiomers (Figure 2). Clearly, in dioxane a self-assembly process occurs, with formation of supramolecular aggregates with opposite helicities for the two enantiomers.

The strong bands at $\lambda = 387$ and 368 nm are assigned to bipyridine transitions,[31,32] while the very broad signal centered at $\lambda = 465$ nm and the shoulder at $\lambda = 319$ nm very probably result from transitions involving the TTF units. These features demonstrate not only that the bipyridine units are tilted in the same sense within the helical stacks but also that the TTF fragments are twisted preferentially, as a result of the favored helicity imposed by the homochiral isopentyl chains. The variable temperature behavior of the CD signal shows that at higher temperatures the aggregates tend to dissociate. Indeed, when heating a solution of **1a** in dioxane ($c = 2 \times 10^{-5}$ M) to 60 °C for a couple of minutes only, a complete loss of the CD signal is observed (Figure 3). Nevertheless, not only is the signal recovered upon cooling the solution back to 20 °C, since an asymptotic growth

dx.doi.org/10.1021/ja202211k | J. Am. Chem. Soc. 2011, 133, 8344–8353

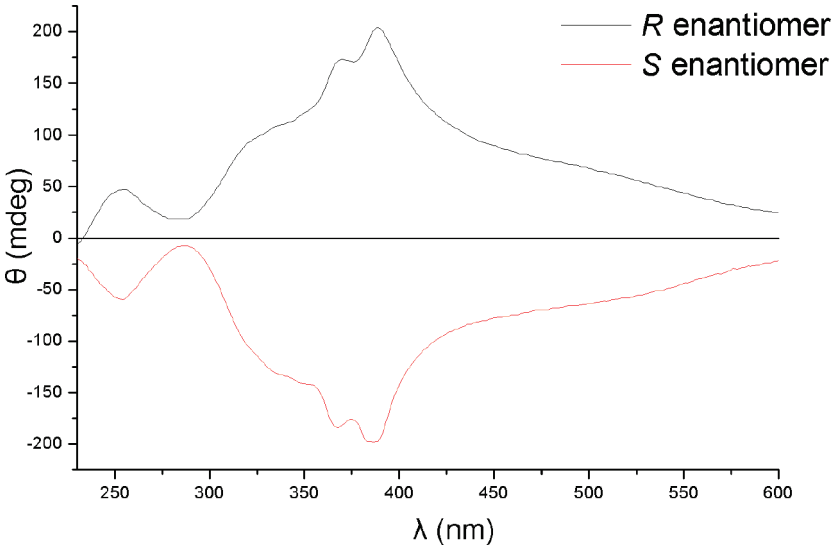

Figure 2. CD spectra of the enantiomers (*S*)-**1a** and (*R*)-**1b** in dioxane ($c = 5 \times 10^{-5}$ M) in a rectangular cell with a 2 mm path length.

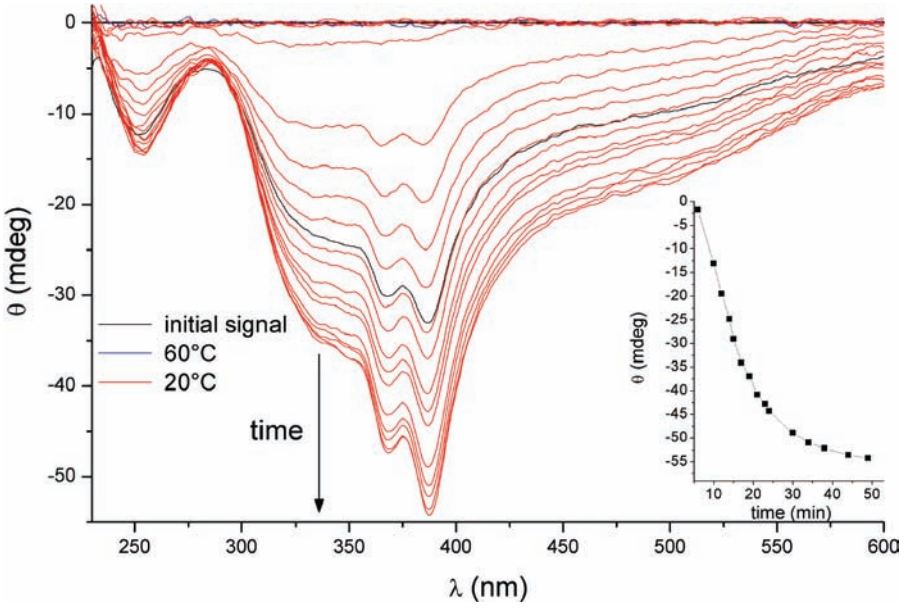

Figure 3. Temperature dependence of the CD spectra in dioxane of (*S*)-**1a** ($c = 2 \times 10^{-5}$ M) in a rectangular cell with a 2 mm path length. Inset: Time dependence of the CD intensity signal at 387 nm after cooling at 20 °C.

with time is observed, but also its intensity becomes much larger than the initial one, showing that in the final solution the aggregates are longer or are better organized because of the slow cooling. We hypothesize that upon heating most of the aggregates were disassembled, and only a fraction of small optically inactive aggregates remained, which act as seeds for the growth of the optically active self-assembled fibers when cooling the solution. This process is reproducible and gives mirror image spectra for the enantiomers, suggesting that any linear dichroism is negligible.

This explanation is supported by the fact that the CD signal is not recovered after heating at 50−60 °C for a couple of minutes for concentrations smaller than 1×10^{-5} M, or for 20 min (and more) for concentrations of 2×10^{-5} M, indicating that the critical concentration for nucleation of the aggregates (i.e., supersaturation) is apparently not reached. So, the aggregates are not formed in 24 h (or more) after total dissolution. However, when a fresh concentrated solution (1×10^{-4} M) is added to the heated and cooled 2×10^{-5} M solution to reach a final concentration of 3.6×10^{-5} M, the CD signal of the resulting mixture is much more intense than the one due only to the nucleation sites provided by the new solution. Therefore, it seems that the existing aggregates from the added solution act as seeds for the self-assembly of the molecules dispersed in the initially heated solution (Figure 4).

A solution prepared with a racemic mixture of **1a** and **1b** does not show any optical activity, as expected, confirming that the effects reported above are not a result of linear dichroism. On the other hand, no clear evidence for a "majority rules" effect could be observed by CD measurements (*vide infra*). That is, a straight line of optical activity versus ratio of enantiomers is obtained.

dx.doi.org/10.1021/ja202211k |*J. Am. Chem. Soc.* 2011, 133, 8344–8353

This again points to the importance of kinetic effects (nucleation and growth) in the formation of the fibers of **1**.

Molecular Modeling of Simple Stacks. In order to get more insight into the self-assembly process and to determine the sense of helicity of the aggregates in solution, molecular mechanics (MM) and molecular dynamics (MD) calculations were performed, while periodic boundary conditions (PBC) were used to simulate infinite stacks. The stabilization energy per molecule arising from stacking interaction is calculated as $E_{stab} = (nE_{isol} - E_{stack})/n$, where n is the number of molecules within the stack, E_{isol} the energy of an isolated molecule, and E_{stack} the energy of the stack. Four systems with increasing complexity were studied, starting from the C_3 core tris[3(3′-formylamino)-2,2′-bipyridyl]-benzene-1,3,5-tricarbonamide, and then by adding successively on the bipyridine wedges TTF, bis(thioethyl)-TTF, and, finally, (*R*)- or (*S*)-2-methylbutylthio-TTF units (Supporting Information). In each case two helices, one clockwise (*CW* or *P*) and the other counter-clockwise (*CCW* or *M*), have been built. While for the first system the twist of the helices converged to about 12.0°, and therefore a periodic box of 10 molecules was sufficient to simulate an infinite stack, when considering the C_3 symmetry of our systems, introduction of TTF units provoked a reduction of the twist to about 8.0°, in order to accommodate TTF···TTF interactions. Consequently, a periodic box of 15 molecules is required to simulate an infinite stack for the TTF containing systems. Obviously, the first three compounds are achiral, and thus the *P* and *M* helices have strictly the same energy (Supporting Information). The introduction of a chiral group (here the (*S*)-methyl-butyl chain) has a drastic influence on the stability, since the two helices (*P* and *M*) are no longer equivalent. Even if the twist of the helix remains unchanged (about 8°), the intermolecular distance between the units within the stack is slightly different, 4.01 Å for the *P* helix and 4.03 Å for the (*M*) helix. More importantly, MD simulations show clearly that the *M* helix is more stable than the *P* helix (Supporting Information). By optimizing several points along the MD trajectory, we were able to calculate the stabilization energy per molecule at 104.8 ± 0.4 kcal/mol for the *P* helix and 106.8 ± 0.5 kcal/mol for the *M* helix, indicating that the *M* primary twisted ribbon is the most stable, very likely thanks to more favorable van der Waals interactions between the chains, and should be the one responsible for the chiroptical signals in the CD spectra in solution. Although the two structures seem similar at first sight, there are clear differences in the arrangement of the (*S*)-methyl-butyl groups at the periphery and also some tiny differences in the hydrogen bond distances between the amide groups and bipyridine moieties (Figure 5).

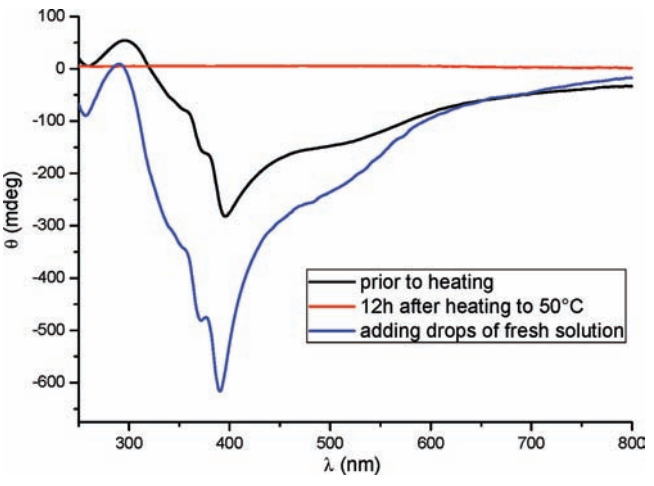

Figure 4. CD spectra in dioxane of (*S*)-**1a** at 20 °C before heating ($c = 2 \times 10^{-5}$ M) (black line), after heating at 50 °C for 20 min and then standing at 20 °C for 12 h ($c = 2 \times 10^{-5}$ M) (red line), and after adding fresh solution ($c_{final} = 3.6 \times 10^{-5}$ M) (blue line), in a rectangular cell with a 10 mm path length.

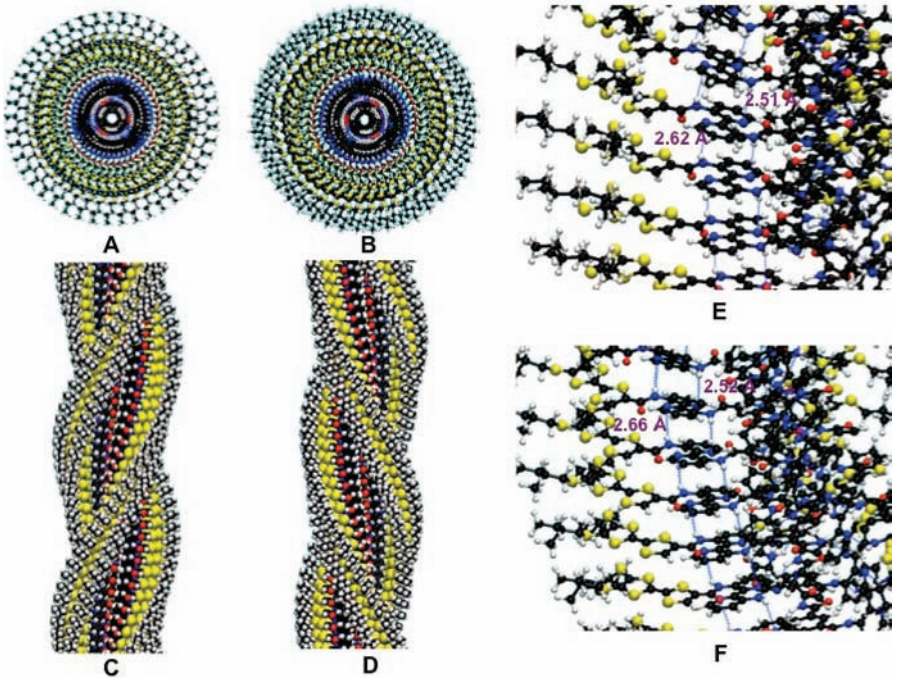

Figure 5. Aggregate of (*S*)-**1a**. Top view (A), side view (C), and detailed view (E) for the *P* helix; top view (B), side view (D), and detailed view (F) for the *M* helix.

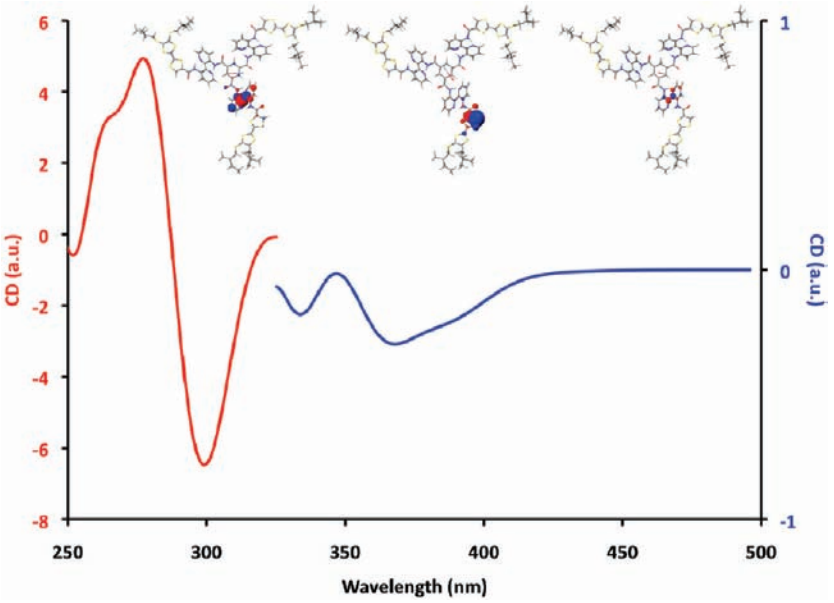

Figure 6. Excitonic CD spectrum of (*S*)-**1a** as averaged over the MD trajectory. The inset shows transition densities for a few relevant molecular electronic transitions involved in the weak, low-energy broad band (B, blue line) and the strong, high-energy band (A, red line). Note the different scales.

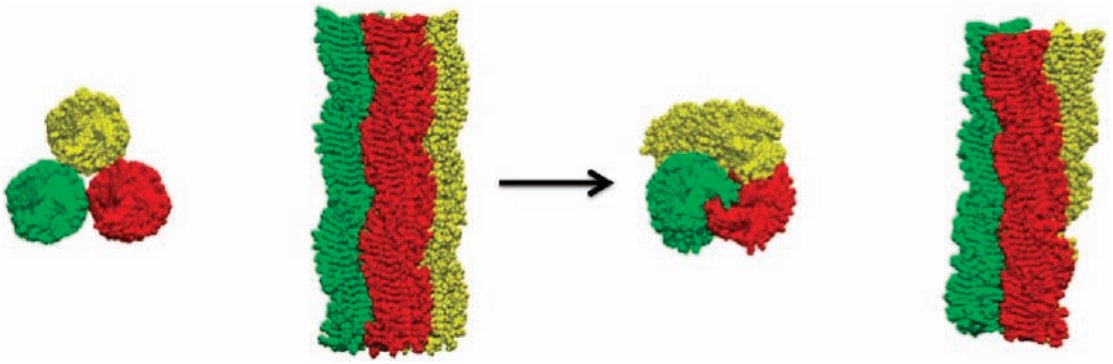

Figure 7. Formation of the coiled superhelix after 100 ps of dynamics.

Note that the calculated diameter of a fiber amounts to 43.3 ± 0.1 Å. The shortest intermolecular S···S contacts within the fibers range between 3.87 and 4.48 Å, at the limit of the van der Waals interactions, while the dihedral angles between the aromatic core and the bipyridine units, and the bipyridine and TTF units, amount to 49.7° and 139.0°, respectively (see Supporting Information). Thus, there is clearly an interplay between the $\pi-\pi$ stacking of the aromatic units, TTF···TTF interactions, and hydrogen bonding between the amide groups responsible for the formation and stability of these primary fibers.

Snapshots extracted along the MD simulations of an (*S*)-**1a** (*M*) helix were used as input for the calculation of the excitonic contribution to the CD response (see Experimental Section). The results reported in Figure 6 show multiple negative CD bands consistent with a left-handed chiral arrangement of the chromophores. Transitions with weak optical and CD intensity are predicted in the range 450−350 nm that have contributions from both TTF and bipyridine localized electronic excitations, while a much stronger bipyridine band is computed at ∼300 nm. This assignment is consistent with the analysis of the measured absorption and CD spectra above, yet the calculated transitions are blue-shifted by about 60−90 nm compared to experiment (likely because solvent effects were not taken into account in the calculations).

Note that this is the first time in this type of C_3 symmetric systems when the helical conformation (*M* or *P*) of the aggregates in solution has been unambiguously determined on the basis of experimental and theoretical CD combined with MM and MD simulations. Obviously, the opposite result is obtained when the simulation is performed with the (*R*)-methyl-butyl chain, that is a more stable P conformation by 2 kcal/mol (8.38 kJ/mol) per molecule. In order to estimate the effect of introducing a small amount of the "wrong" enantiomer into a stack formed by the major enantiomer in its preferred helical sense, two *M* helices containing either 14 (*S*)-**1a** and 1 (*R*)-**1b** molecules or 13 (*S*)-**1a** and 2 noninteracting (*R*)-**1b** molecules have been optimized. In the first case the aggregate is 0.3 kcal/mol (1.26 kJ/mol) per molecule less stable than the all (*S*) stack, while in the second case it is already 1 kcal/mol less stable, thus indicating that the sequential insertion of the opposite enantiomer within a chain of a major enantiomer does not have a linear effect. This could explain the nonexistence of a "majority rules" effect in our system, since for an ee of 73%, corresponding to a stack with 13 (*S*)-**1a** and

dx.doi.org/10.1021/ja202211k | *J. Am. Chem. Soc.* 2011, 133, 8344–8353

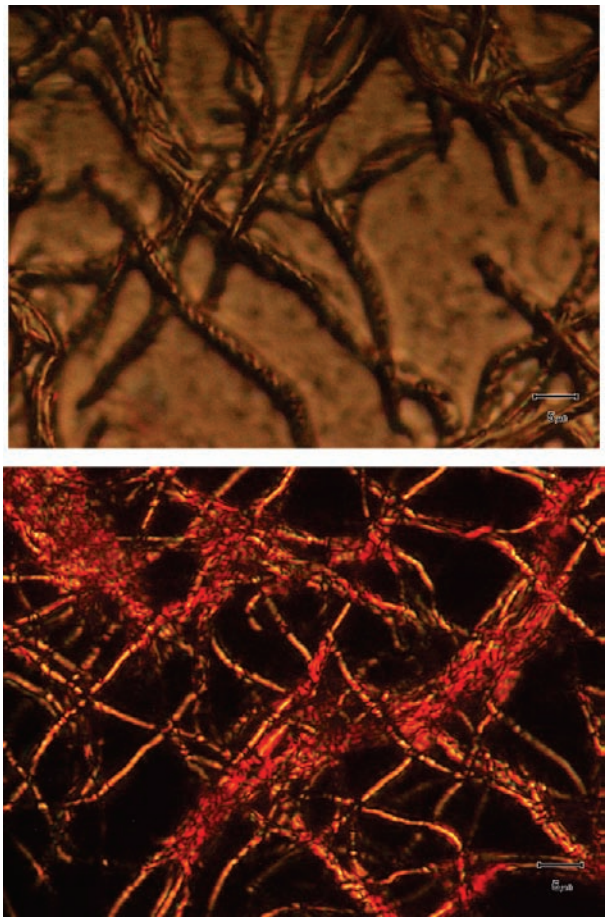

Figure 8. Optical micrographs (above) in reflection mode of the *P* helical fibers obtained from a solution of (*S*)-**1a** (2 mg/mL) in dioxane and (below) in transmission with polarizing filters crossed.

2 (*R*)-**1b** molecules, the chain is already at the halfway point to the helix reversal in terms of energy (105.8 kcal/mol) when compared to the pure chain of 15 (*S*)-**1a** molecules (106.8 kcal/mol in *M* and 104.8 kcal/mol in *P* conformations). To gain insight into the upper level of organization of the system, three primary fibers built out of 45 (*S*)-**1a** molecules, in an *M* conformation, have been set next to each other and then left free to self-assemble with no imposed constraint. MD simulations (100 ps) clearly show that the three helices wrap spontaneously one around the other to converge to a coiled superhelix of the *M* conformation (Figure 7). The diameter of this secondary helix is around 6−7 nm. The estimated shortest S···S distance between neighboring fibers amounts to about 7.8 Å.

Hierarchical Self-Assembly. As pointed out above, CD measurements have been performed at concentrations for **1** in dioxane of 10^{-5} M, for which no precipitation occurred. However, at higher concentrations the compound can be dissolved in dioxane by heating for a longer time, but upon cooling back to room temperature a precipitate slowly appears. The analysis of this precipitate by optical or scanning electronic microscopy (SEM) reveals the formation of fibers with an exceptionally well-defined mesoscale helicity, which can be clearly visualized by these techniques. The best quality fibers were formed for concentrations in **1a**−**b** of 2 mg/mL (1×10^{-3} M), and as can be observed in Figure 8, the fibers, obtained from the (*S*) enantiomer **1a**, show right-handed (*P*) helicity. The fibers are as

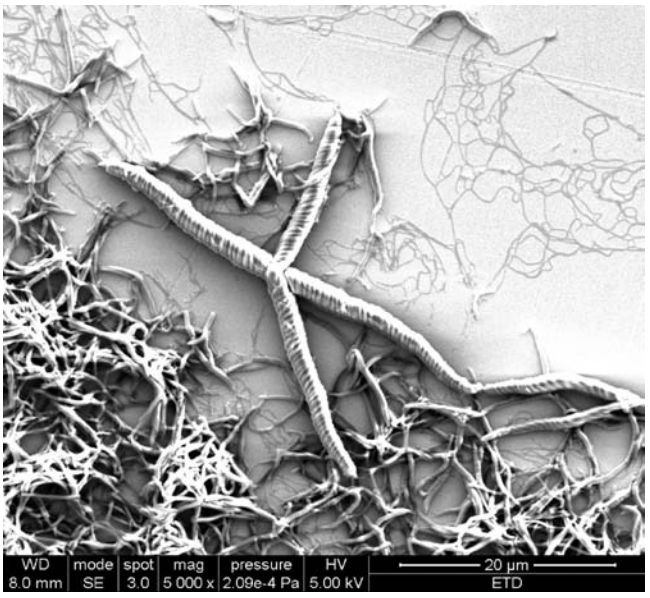

Figure 9. SEM image of the *P* helical fibers with different sizes obtained from a solution of (*S*)-**1a** (2 mg/mL) in dioxane and deposited on gold on glass, with no coating.

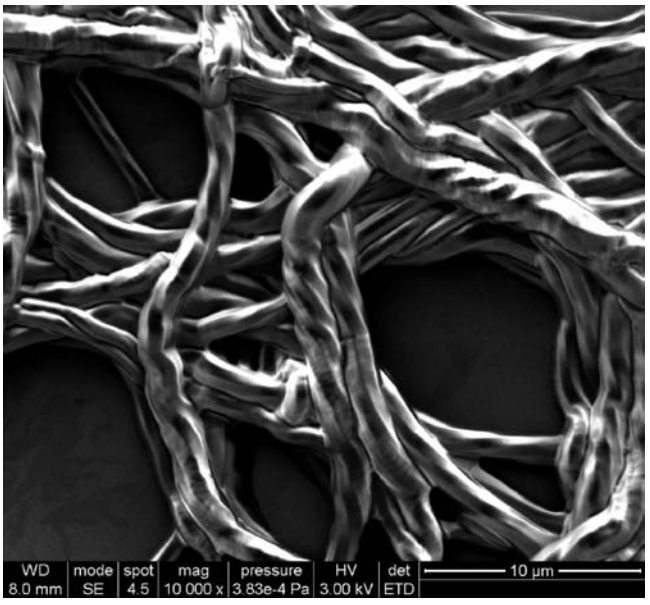

Figure 10. SEM image of the (*M*) helical fibers obtained from a solution of (*R*)-**1b** (2 mg/mL) in dioxane and deposited on gold on glass, with no coating.

long as dozens of micrometers, while their height is identical to their width, amounting to 1.5−2.0 μm, as proven by changing the focal plane from the top of the fibers to the middle, and to the bottom. In addition, the molecules seem to be well ordered in the fibers, as indicated by the bright contrast seen in transmission optical micrographs.

Measurement of the sizes of the fibers in the sharpest images indicates that they have a thickness of about 1.5−1.6 μm. The stripes visible on the fibers have a thickness of 1.05−1.1 μm, form an angle of 45° with the long axis of the fiber, and repeat with a pitch of 1.05 μm. It appears thus that the large fiber is formed

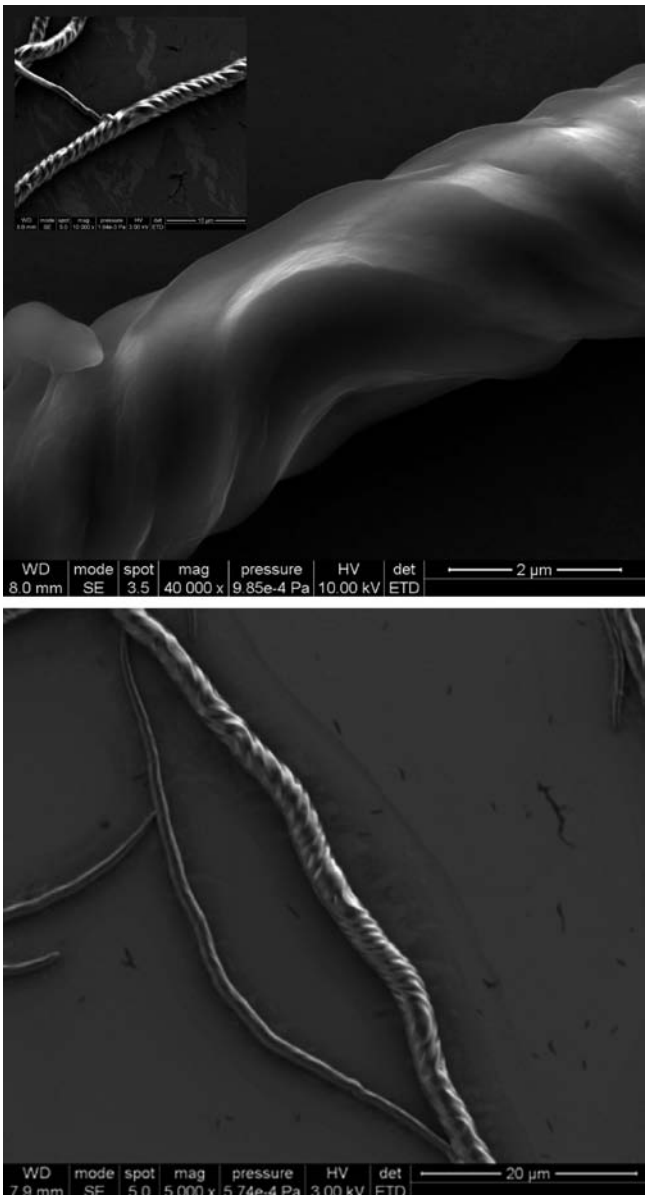

Figure 11. SEM images of helical fibres obtained from a sample of 1:1 (*S*)-**1a**/(*R*)-**1b** (2 mg/mL each) in dioxane and deposited on gold on glass, with no coating.

from two smaller ones that twist around each other. When considering the computed diameter (~4.3 nm) of a primary fiber it appears that (at least) approximately 250 primary helices could fit side by side in one of these smaller fibers visible as stripes on the big fiber, yet this number should be much larger since the single fibers twist around each other when put close together, as observed in the simulation with three of them. The fibers are bright in the polarized transmission optical micrographs, indicating a highly ordered and periodic superstructure. At first sight, the inversion of helicity between the primary twisted stacks or secondary helical aggregates of *M* conformation in solution and the solid fibers, which can be seen as superhelices or supercoiled coils formed upon hierarchical self-assembling at successive levels of organization, seems surprising. Nevertheless, various examples of helical architectures, either synthetic, as those described by Nolte et al.,[53−56] or from nature, such as the famous example of the collagen,[57−59] consisting of three left-handed helices giving rise by self-assembly to a right-handed coiled coil, show the same type of helical inversion between the different levels of hierarchical organization, although it is very difficult to rationalize or to predict this behavior. The following image (Figure 9) shows an area with larger fibers seen very occasionally, which show a higher order of chiral expression, but of the same sense. These fibers have a width of 2.5 μm, whereas the majority of the fibers have a width of 1.5−2.0 μm. As expected, the (*R*) enantiomer **1b** provides fibers with the opposite helicity (*M*) but the same size range, under the same conditions (Figure 10).

When a racemic mixture of (*S*)-**1a** (2 mg/mL) and (*R*)-**1b** (2 mg/mL) is reprecipitated from hot dioxane the pattern of the fibers is particularly interesting, since within the same fiber there are several homochiral but opposite domains with points where helical reversal is clearly observed (Figure 11).

The size of these fibers is similar to that of the enantiopure ones. The fact that helical reversal is observed in the case of the racemic mixture can be discussed in terms of a diffusion controlled process. For example, during the formation of the fibers from (*S*)-**1a**, with (*P*) helicity, the growth rate is far superior to the diffusion rate, thus leading to a gradual increase of the local supersaturation in the opposite enantiomer (*R*) until the point when the critical supersaturation is reached. Then the growth of the fiber continues with the (*R*) enantiomer which promotes the opposite helicity (*M*) after an occurrence of helical reversal. Thus, the formation of fibers resembles an oscillating process and can be related to the 2D oscillating crystallization phenomenon, nicely described by Coquerel et al.[60] This idea is backed up by the observation of much longer but less ordered fibers upon mechanical stirring during precipitation, very likely because of the faster kinetics favoring the diffusion process. Variable ratio mixtures of the two enantiomers did also provide the same type of fibers showing both helicities, with no indication of a "majority rules" effect, in agreement with the CD measurements and the MM and MD simulations on the primary fibers.

CONCLUSIONS

Enantiopure C_3 symmetric disk-shaped molecules containing electroactive TTF units decorated with short chiral isopentyl chains can be synthesized effectively, and they self-assemble into helical aggregates showing a preferential helicity twist over several length scales. In solution, the formation of primary helices as twisted stacks is investigated by CD measurements combined with theoretical calculations. The CD investigations show that the chiral expression can be improved by thermal dissociation and reformation on a nucleus in the solution and that the growth of the fibers is controlled by the nucleation event. The relative stability of the (*P*) and (*M*) conformations of the stacks has been evaluated by MM and MD simulations, which clearly indicate that the (*S*)-**1a** enantiomer provides the *M* helix, more stable by 2 kcal/mol per molecule than the *P* helix, in agreement with the optical activity observed in CD spectra. Also, a simulation of a stack containing a large majority of one enantiomer and one or two molecules of the opposite enantiomer shows that the insertion of the "wrong" enantiomer in the helix is unfavorable for the observation of the "majority rules" effect, in the sense that the energy difference between the two helical twists becomes much smaller. For higher concentrations of the compound mesoscopic size chiral fibers have been obtained, their formation being clearly dependent on seeding nucleation and diffusion rate.

Optical and electron microscopy studies show that the solid fibers, comprised of multiple fibers, have opposite chirality with respect to the helicity of the single strand fibers in solution. Remarkable morphologies are observed for the fibers obtained with the racemic mixture, since homochiral domains together with helical reversal points are present within the same fiber. Thus, these TTF-containing C_3 symmetric compounds allowed the achievement of an unprecedented hierarchical chiral self-assembly in a nonamphiphilic system, very likely thanks to the propensity of the TTF units to engage in intermolecular S···S contacts. These results open up many possibilities regarding the modulation of the helical pitch as a function of the chiral group attached to the perimeter of the molecule, and hence the self-assembly properties, as an important step toward the elaboration of conducting mesoscopic helical supramolecular fibers. They may be useful for transcription into inorganic materials[61] and are interesting in the context of other recent observations of chiral morphology[62] which are not necessarily seen in aggregates of chiral disk-like compounds with different numbers of stereogenic centers.[63]

In the present case, the importance of nucleation in the growth of chiral fibers can be monitored using CD spectroscopy, which opens an opportunity for the study of this phenomenon in this and related systems which show hierarchical growth and where nucleation plays a key role.

■ ASSOCIATED CONTENT

Supporting Information. Full experimental section including description of the synthesis and characterization of all new materials and all the techniques employed in the research reported here. This material is available free of charge via the Internet at http://pubs.acs.org.

■ AUTHOR INFORMATION

Corresponding Author
amabilino@icmab.es; narcis.avarvari@univ-angers.fr

■ ACKNOWLEDGMENT

This work was supported in France by the Ministry of Education and Research (grants to I.D. and F.R.), the National Agency for Research (ANR, Project 09-BLAN-0045-01), and the CNRS, in Spain by the DGI-Spain (Project CTQ2010-16339), DGR, Catalonia (Project 2009 SGR 158), and the European Community's Seventh Framework Programme under Grant Agreement No. NMP4-SL-2008-214340, Project RESOLVE. Financial support from the COST Action D35 is also gratefully acknowledged. The work in Mons is partly supported by the Interuniversity Attraction Pole IAP 6/27 of the Belgian Federal Government and the Belgian National Fund for Scientific Research (FNRS/FRFC). D.B. is a FNRS Research Director.

■ REFERENCES

(1) Wagnière, G. H. *On Chirality and the Universal Asymmetry*; Wiley-VCH: Weinheim, 2007.
(2) Brizard, A.; Oda, R.; Huc, I. *Top. Curr. Chem.* **2005**, *256*, 167–218.
(3) Crego-Calama, M.; Reinhoudt, D. N. *Supramolecular Chirality. Topics in Current Chemistry*; Springer: Berlin, Heidelberg, NY, 2006.
(4) Amabilino, D. B. *Chirality at the Nanoscale*; Wiley-VCH: Weinheim, 2009.
(5) de Loos, M.; van Esch, J.; Kellogg, R. M.; Feringa, B. L. *Angew. Chem., Int. Ed.* **2001**, *40*, 613–616.
(6) Sato, I.; Kadowaki, K.; Urabe, H.; Jung, J. H.; Ono, Y.; Shinkai, S.; Soai, K. *Tetrahedron Lett.* **2003**, *44*, 721–724.
(7) Jung, J. H.; Ono, Y.; Hanabusa, K.; Shinkai, S. *J. Am. Chem. Soc.* **2000**, *122*, 5008–5009.
(8) Ringler, P.; Müller, W.; Ringsdorf, H.; Brisson, A. *Chem.—Eur. J.* **1997**, *3*, 620–625.
(9) Wilson-Kubalek, E. M.; Brown, R. E.; Celia, H.; Milligan, R. A. *Proc. Natl. Acad. Sci. U.S.A.* **1998**, *95*, 8040–8045.
(10) Hartgerink, J. D.; Beniash, E.; Stupp, S. I. *Proc. Natl. Acad. Sci. U.S.A.* **2002**, *99*, 5133–5138.
(11) Xia, Y.; Yang, P.; Sun, I.; Wu, Y.; Mayers, B.; Gates, B.; Yin, Y.; Kim, F.; Yan, H. *Adv. Mater.* **2003**, *15*, 353–389.
(12) van Bommel, K. J. C.; Friggeri, A.; Shinkai, S. *Angew. Chem., Int. Ed.* **2003**, *42*, 980–999.
(13) Yang, Y.; Nakazawa, M.; Suzuki, M.; Shirai, H.; Hanabusa, K. *J. Mater. Chem.* **2007**, *17*, 2936–2943.
(14) Palmans, A. R. A.; Meijer, E. W. *Angew. Chem., Int. Ed.* **2007**, *47*, 8948–8968.
(15) Pijper, D.; Feringa, B. L. *Soft Matter* **2008**, *4*, 1349–1372.
(16) Praveen, V. K.; Babu, S. S.; Vijayakumar, C.; Varghese, R.; Ajayaghosh, A. *Bull. Soc. Chem. Jpn.* **2008**, *81*, 1196–1211.
(17) Lee, C. C.; Grenier, C.; Meijer, E. W.; Schenning, A. P. H. J. *Chem. Soc. Rev.* **2009**, *38*, 671–683.
(18) Sijbesma, R. P.; Meijer, E. W. *Chem. Commun.* **2003**, 5–16.
(19) Schenning, A. P. H. J.; Jonkheijm, P.; Peeters, E.; Meijer, E. W. *J. Am. Chem. Soc.* **2001**, *123*, 409–416.
(20) Jonkheijm, P.; van der Schoot, P.; Schenning, A. P. H. J.; Meijer, E. W. *Science* **2006**, *313*, 80–83.
(21) Schoonbeek, F. S.; van Esch, J. H.; Wegewijs, B.; Rep, D. B. A.; de Haas, M. P.; Klapwijk, T. M.; Kellogg, R. M.; Feringa, B. L. *Angew. Chem., Int. Ed.* **1999**, *38*, 1393–1397.
(22) Rep, D. B. A.; Roelfsema, R.; van Esch, J. H.; Schoonbeek, F. S.; Kellogg, R. M.; Feringa, B. L.; Palstra, T. T. M.; Klapwijk, T. M. *Adv. Mater.* **2000**, *12*, 563–566.
(23) Jin, W.; Yamamoto, Y.; Fukushima, T.; Ishii, N.; Kim, J.; Kato, K.; Takata, M.; Aida, T. *J. Am. Chem. Soc.* **2008**, *130*, 9434–9440.
(24) Yamamoto, T.; Fukushima, T.; Kosaka, A.; Jin, W.; Yamamoto, Y.; Ishii, N.; Aida, T. *Angew. Chem., Int. Ed.* **2008**, *47*, 1672–1675.
(25) Hasegawa, M.; Iyoda, M. *Chem. Soc. Rev.* **2010**, *39*, 2420–2427.
(26) Schenning, A. P. H. J.; Meijer, E. W. *Chem. Commun.* **2005**, 3245–3258.
(27) Hoeben, F. J. M.; Jonkheijm, P.; Meijer, E. W.; Schenning, A. P. H. J. *Chem. Rev.* **2005**, *105*, 1491–1546.
(28) Palmans, A. R. A.; Vekemans, J. A. J. M.; Fischer, H.; Hikmet, R. A.; Meijer, E. W. *Chem.—Eur. J.* **1997**, *3*, 300–307.
(29) Brunsveld, L.; Zhang, H.; Glasbeek, M.; Vekemans, J. A. J. M.; Meijer, E. W. *J. Am. Chem. Soc.* **2000**, *122*, 6175–6182.
(30) van Gorp, J. J.; Vekemans, J. A. J. M.; Meijer, E. W. *J. Am. Chem. Soc.* **2002**, *124*, 14759–14769.
(31) Palmans, A. R. A.; Vekemans, J. A. J. M.; Havinga, E. E.; Meijer, E. W. *Angew. Chem., Int. Ed. Engl.* **1997**, *36*, 2648–2651.
(32) van Gestel, J.; Palmans, A. R. A.; Titulaer, B.; Vekemans, J. A. J. M.; Meijer, E. W. *J. Am. Chem. Soc.* **2005**, *127*, 5490–5494.
(33) van Houtem, M. H. C. J.; Martín-Rapún, R.; Vekemans, J. A. J. M.; Meijer, E. W. *Chem.—Eur. J.* **2010**, *16*, 2258–2271.
(34) Palmans, A. R. A.; Vekemans, J. A. J. M.; Hikmet, R. A.; Fischer, H.; Meijer, E. W. *Adv. Mater.* **1998**, *10*, 873–876.
(35) Gottarelli, G.; Lena, S.; Masiero, S.; Pieraccini, S.; Spada, G. P. *Chirality* **2008**, *20*, 471–485.
(36) Green, M. M.; Peterson, N. C.; Sato, T.; Teramoto, A.; Cook, R.; Lifson, S. *Science* **1995**, *268*, 1860–1866.
(37) Segura, J. L.; Martin, N. *Angew. Chem., Int. Ed.* **2001**, *40*, 1372–1401.
(38) Canevet, D.; Sallé, M.; Zhang, G.; Zhang, D.; Zhu, D. *Chem. Commun.* **2009**, 2245–2269.

(39) Danila, I.; Riobé, F.; Puigmarti-Luis, J.; Pérez del Pino, Á.; Wallis, J. D.; Amabilino, D. B.; Avarvari, N. *J. Mater. Chem.* **2009**, *19*, 4495–4504.
(40) Akutagawa, T.; Kakiuchi, K.; Hasegawa, T.; Noro, S.; Nakamura, T.; Hasegawa, H.; Mashiko, S.; Becher, J. *Angew. Chem., Int. Ed.* **2005**, *44*, 7283–7287.
(41) Kitahara, T.; Shirakawa, M.; Kawano, S.; Beginn, B.; Fujita, N.; Shinkai, S. *J. Am. Chem. Soc.* **2005**, *127*, 14980–14981.
(42) Kitamura, T.; Nakaso, S.; Mizoshita, N.; Tochigi, Y.; Shimomura, T.; Moriyama, M.; Ito, K.; Kato, T. *J. Am. Chem. Soc.* **2005**, *127*, 14769–14775.
(43) Puigmartí-Luis, J.; Minoia, A.; Pérez del Pino, A.; Ujaque, G.; Rovira, C.; Lledós, A.; Lazzaroni, R.; Amabilino, D. B. *Chem.—Eur. J.* **2006**, *12*, 9161–9175.
(44) Puigmartí-Luis, J.; Laukhin, V.; Pérez del Pino, A.; Vidal-Gancedo, J.; Rovira, C.; Laukhina, E.; Amabilino., D. B. *Angew. Chem., Int. Ed.* **2007**, *46*, 238–241.
(45) Puigmartí-Luis, J.; Pérez del Pino, A.; Laukhina, E.; Esquena, J.; Laukhin, V.; Rovira, C.; Vidal-Gancedo, J.; Kanaras, A. G.; Nichols, R. J.; Brust, M.; Amabilino, D. B. *Angew. Chem., Int. Ed.* **2008**, *47*, 1861–1865.
(46) Ahn, S.; Kim, Y.; Beak, S.; Ishimoto, S.; Enozawa, H.; Isomura, E.; Hasegawa, M.; Iyoda, M.; Park, Y. *J. Mater. Chem.* **2010**, *20*, 10817–10823.
(47) Tatewaki, Y.; Hatanaka, T.; Tsunashima, R.; Nakamura, T.; Kimura, M.; Shirai, H. *Chem.—Asian J.* **2009**, *4*, 1474–1479.
(48) Walkup, R. D.; Boatman, P. D., Jr.; Kane, R. R.; Cunningham, R. T. *Tetrahedron Lett.* **1991**, *32*, 3937–3940.
(49) Nakajima, N.; Horita, K.; Abe, R.; Yonemitsu, O. *Tetrahedron Lett.* **1988**, *29*, 4139–4142.
(50) Reiss, T.; Breit, B. *Org. Lett.* **2009**, *11*, 3286–3289.
(51) Rice, C. R.; Onions, S.; Vidal, N.; Wallis, J. D.; Senna, M.-C.; Pilkington, M.; Stoeckli-Evans, H. *Eur. J. Inorg. Chem.* **2002**, 1985–1997.
(52) Baudron, S. A.; Avarvari, N.; Canadell, E.; Auban-Senzier, P.; Batail, P. *Chem.—Eur. J.* **2004**, *10*, 4498–4511.
(53) Cornelissen, J. J. L. M.; Fischer, M.; Sommerdijk, N. A. J. M.; Nolte, R. J. M. *Science* **1998**, *280*, 1427–1430.
(54) Engelkamp, H.; Middelbeek, S.; Nolte, R. J. M. *Science* **1999**, *284*, 785–788.
(55) Sommerdijk, N. A. J. M.; Buynsters, P. J. J. A.; Akdemir, H.; Geurts, D. G.; Pistorius, A. M. A.; Feiters, M. C.; Nolte, R. J. M.; Zwanenburg, B. *Chem.—Eur. J.* **1998**, *4*, 127–136.
(56) Elemans, J. A. A. W; Rowan, A. E.; Nolte, R. J. M. *J. Mater. Chem.* **2003**, *13*, 2661–2670.
(57) Ramachandran, G. N.; Kartha, G. *Nature* **1955**, *176*, 593–595.
(58) Rich, A.; Crick, F. H. C. *Nature* **1955**, *176*, 915–916.
(59) Bhattacharjee, A.; Bansal, M. *IUBMB Life* **2005**, *57*, 161–172.
(60) Gervais, C.; Beilles, S.; Cardinaël, P.; Petit, S.; Coquerel, G. *J. Phys. Chem. B* **2002**, *106*, 646–65.
(61) Arnal-Herault, C.; Banu, A.; Barboiu, M.; Michau, M.; van der Lee, A. *Angew. Chem., Int. Ed.* **2007**, *46*, 4268–4272.
(62) Aparicio, F.; Vicente, F.; Sanchez, L. *Chem. Commun.* **2010**, 8356–8358.
(63) Iavicoli, P.; Xu, H.; Feldborg, L. N.; Linares, M.; Paradinas, M.; Stafström, S.; Ocal, C.; Nieto-Ortega, B.; Casado, J.; López Navarrete, J. T.; Lazzaroni, R.; De Feyter, S.; Amabilino, D. B. *J. Am. Chem. Soc.* **2010**, *132*, 9350–9362.